Research Square

Preprints are preliminary reports that have not undergone peer review.
They should not be considered conclusive, used to inform clinical practice,
or referenced by the media as validated information.

Hydrometallurgical synthesis and comprehensive characterization of alumina copper composites from black aluminium dross for enhanced application performance

Sathiyaseelan G
Sri Ramakrishna engineering college
Bhagyanathan C
sathiyaseelan.g@srec.ac.in

Sri Ramakrishna engineering college
Sinath P
Sri Ramakrishna engineering college
Gottmyers Melwyn J
Sri Ramakrishna engineering college

Research Article

Keywords: Advanced Characterization, Structural Integrity, Optical Properties, Aluminium Dross Valorisation, Coating suitability

Posted Date: May 13th, 2026

DOI: https://doi.org/10.21203/rs.3.rs-9433290/v1

License: This work is licensed under a Creative Commons Attribution 4.0 International License.
Read Full License

Additional Declarations: No competing interests reported.

Abstract

The conversion of aluminium dross into value-added functional materials requires a rigorous evaluation of properties relevant to surface engineering applications. In this study, we present a continuation of our previously developed hydrometallurgical route, focusing exclusively on the synthesis and advanced characterisation of an alumina-copper composite to assess its suitability for coating applications. An alumina-copper composite with a 9:1 weight ratio was synthesised through a redox-assisted process followed by controlled ball milling to ensure compositional homogeneity and refined particle dispersion. Advanced characterisation techniques, including particle size analysis and dynamic light scattering, thermogravimetric–differential scanning calorimetry, ultraviolet-visible spectroscopy, high-resolution transmission electron microscopy, X-ray photoelectron spectroscopy, and Brunauer-Emmett-Teller surface area analysis, were employed to systematically evaluate particle dispersion, thermal stability, surface chemistry, and textural properties. The results demonstrate that the composite exhibits fine particle size distribution, high thermal stability, and favourable surface and interfacial characteristics, which are critical prerequisites for coating formulation and deposition. This study provides a comprehensive materials-level assessment that establishes the alumina-copper composite as a promising candidate for coating development, while laying the groundwork for future performance-based evaluation.

1) INTRODUCTION

The efficient utilization of aluminium dross, a byproduct from aluminium melting processes, remains a critical challenge due to its composition of valuable metal residues and oxides [1–5]. Conventional methods, including pyrometallurgical techniques and physical separation, often struggle with limited recovery rates and high energy demands, thus failing to fully capitalise on the dross's potential [6, 7]. In contrast, hydrometallurgical processes, which utilise aqueous solutions to extract and recover valuable elements, present a more sustainable and effective approach. These techniques not only improve resource recovery but also reduce environmental impact compared to traditional methods [8–10]. This research extends previous work by investigating the hydrometallurgical synthesis of alumina-copper composites derived from black aluminium dross[3]. The composite, featuring a 9:1 alumina-to-copper ratio, is produced through a redox and reprecipitation reaction followed by ball milling. The preparation process begins with the extraction of aluminium and copper from the dross, which is then subjected to a redox reaction to form a homogeneous mixture. The subsequent ball milling ensures uniform distribution and fine particle size, essential for optimal coating performance. Previous studies on composite preparation highlighted the importance of achieving a uniform morphology and particle size distribution, which are critical for enhancing the composite's performance [11].

The alumina-copper composite benefits from the combined properties of its components: alumina provides high thermal stability and hardness, while copper contributes excellent electrical conductivity. Furthermore, wear resistance and hardness are crucial properties for coatings in high-performance applications such as the aerospace and automotive industries. The alumina phase, known for its high

hardness and mechanical strength, is expected to impart excellent resistance to mechanical wear, while the fine particle distribution of the composite contributes to smooth, defect-free coatings that further enhance durability [12–15]. These attributes together create a material ideal for industrial coatings, offering enhanced durability and resistance to harsh conditions. Compared to traditional pyrometallurgical methods, the hydrometallurgical approach offers reduced energy consumption and lower emissions [16–19]. To thoroughly evaluate the composite's properties, a range of advanced characterization techniques was employed [20–23]. Scanning electron microscopy with energy-dispersive X-ray spectroscopy (SEM-EDX) provided detailed insights into the composite's morphology and elemental composition. Dynamic light scattering (DLS) and particle size analysis (PSA) assessed the particle size distribution [3], while thermogravimetric analysis-differential scanning calorimetry (TG-DSC) evaluated thermal stability. Additionally, zeta potential analysis was performed to assess the stability of the composite suspension, which is crucial for understanding its behaviour in various applications. Further characterisation included ultraviolet-visible (UV-Vis) spectroscopy, high-resolution transmission electron microscopy (HR-TEM), X-ray photoelectron spectroscopy (XPS), and Brunauer-Emmett-Teller (BET) surface area analysis. These methods collectively offer a comprehensive understanding of the composite’s thermal, structural, and rheological properties, demonstrating its suitability for advanced coating applications [24–28].

Earlier studies on alumina-based composites have reported enhanced wear resistance and hardness due to the intrinsic structural stability of alumina [13, 29]. However, the present work does not directly evaluate mechanical or tribological performance. Instead, the focus of this study is limited to the physicochemical characterisation of the synthesised alumina–copper composite. The observed fine particle size distribution (75–180 nm) and relatively uniform dispersion suggest favourable microstructural characteristics that are typically considered advantageous in coating formulations. These features may contribute to improved packing density, dispersion stability, and surface interaction in coating systems. Additionally, the confirmed thermal stability and controlled surface area indicate structural robustness under elevated temperatures. While these characteristics demonstrate material-level suitability for coating-related applications, direct assessment of wear resistance, hardness, and mechanical durability was not performed and remains the subject of future investigation.

2) MATERIALS &METHODS

Materials

This research focuses on the synthesis of alumina-copper composites derived from black aluminium dross through a hydrometallurgical process. The composite material, characterised by a 9:1 ratio of alumina to copper, represents an advancement over previous work in this area. The black aluminium dross, a by-product from aluminium production, serves as the starting material for this study. The hydrometallurgical treatment of this dross facilitates the extraction and refinement of alumina and copper, which are then combined in the specified ratio to produce the composite. This methodology aims to optimise the composite’s properties for potential applications in coating technologies.

Methodology:

Characterisation of the synthesised alumina copper (Al_2O_3-Cu) composites was performed using a combination of structural, spectroscopic, thermal, microscopic, and surface area analysis techniques. Fourier-transform infrared (FTIR) spectra were recorded on a Bruker Alpha FTIR spectrometer (Bruker Optik GmbH, Germany) in the wavenumber range of 400–4000 cm^{-1} with a resolution of 4 cm^{-1} in ATR mode. Thermal stability and decomposition behaviour were analysed using simultaneous thermogravimetric–differential scanning calorimetry (TG-DSC) (NETZSCH STA 449 F3 Jupiter, Germany) under a nitrogen atmosphere at a heating rate of 10°C min^{-1} from room temperature to 1000°C.

Microstructural and morphological investigations were carried out using high-resolution transmission electron microscopy (HR-TEM) (JEOL JEM-2100, operated at 200 kV). Surface chemical states were analysed using X-ray photoelectron spectroscopy (XPS) (Thermo Scientific K-Alpha, USA) employing monochromatic Al Kα radiation (1486.6 eV).

Surface area and porosity characteristics were determined using nitrogen adsorption–desorption measurements performed on a Micromeritics ASAP 2020 surface area analyser (USA) at 77 K. Before analysis, samples were degassed at 200°C for 4 h under vacuum. Specific surface area was calculated using the Brunauer-Emmett-Teller (BET) method, while pore size distribution was evaluated using Brunauer–Emmett–Teller (BET), Barrett–Joyner–Halenda (BJH) pore size distribution, Density Functional Theory (DFT) pore analysis, and thickness plot (t-plot) methods.

Together, these complementary characterisation techniques enabled comprehensive evaluation of the structural, morphological, chemical, thermal, and textural properties of the synthesised alumina–copper composite, supporting its suitability for protective coating applications requiring controlled particle size, uniform dispersion, thermal stability, and optimised surface characteristics

3) RESULT AND DISCUSSION

The hydrometallurgical synthesis of alumina-copper composites from black aluminium dross provides a viable pathway for developing coating precursor materials with controlled physicochemical characteristics. In the present study, suitability for coating applications is evaluated primarily using advanced characterisation techniques, while selected particle size parameters are discussed in relation to previously reported results[3]. As reported in our earlier study, morphological examination using scanning electron microscopy revealed well-dispersed alumina-copper composite particles with limited agglomeration. From a coating perspective, nanoscale particle dimensions and controlled size distribution are critical for achieving uniform film formation and consistent surface coverage. The particle size range and PDI values reported are consistent with those commonly reported for alumina-based composite materials employed in coating formulations[11, 30]. Accordingly, these previously established particle size characteristics provide a foundational basis for the present work, which focuses on advanced physicochemical characterisation to further assess coating suitability.

3.1 Particle Size Analyser (PSA)

Particle size analysis is a critical parameter in evaluating the suitability of alumina-copper composites for coating applications, as particle size distribution strongly influences coating formulation, deposition behaviour, and surface uniformity. Precise control over particle size is particularly important when coatings are applied to aluminium alloy substrates, where uniform particle dispersion contributes to consistent film formation and improved interfacial contact. As reported in our previous study[3]Particle size analysis (PSA) and dynamic light scattering measurements of the alumina-copper composite indicated a fine particle size distribution in the range of 75–180 nm, with an average particle size of approximately 180 nm and a polydispersity index (PDI) of 0.3. These values indicate moderate particle size uniformity, which is generally desirable for coating precursor materials. Similar particle size ranges have been reported to facilitate homogeneous coating layers with reduced defect density in alumina-based composite systems [31–33].

Moreover, alumina-based composites with controlled nanoscale particle distributions tend to exhibit enhanced resistance to deformation and surface damage due to improved load transfer and particle–matrix interaction[34]. Accordingly, the particle size distribution indicates the presence of particles within the measured range, providing information about the dispersion and size uniformity of the synthesised composite. Although direct measurements of hardness and wear resistance are required for quantitative validation of performance.

3.2 SPECTROSCOPIC ANALYSIS

3.2.1 Fourier Transform Infrared Spectroscopy Analysis:

Fourier Transform Infrared Spectroscopy (FTIR) was employed to examine the chemical bonding and functional groups present in the synthesised alumina–copper composite. The FTIR spectrum (Fig. 1), recorded in the range of 400–4000 cm^{-1}, exhibits characteristic absorption bands associated with alumina and copper-containing species. A broad absorption band observed in the region of 3200–3600 cm^{-1}, centred around ~ 3443 cm^{-1}, corresponds to O-H stretching vibrations arising from surface hydroxyl groups or physiosorbed moisture, which are commonly reported for alumina-based materials processed through aqueous routes [23–24]. A pronounced band at ~ 1420 cm^{-1} corresponds to Al-O bending vibrations, confirming the formation of an alumina framework. Additional characteristic absorption bands at ~ 1022 cm^{-1} and ~ 878 cm^{-1}(800–900) are assigned to Al-O stretching and lattice vibrations, respectively, further validating the presence of an alumina-rich phase within the composite. [23–35]. Although metallic copper does not exhibit infrared-active vibrations and therefore cannot be directly detected by FTIR, the presence of copper in the composite is indirectly supported by the absorption feature observed in the lower wavenumber region near ~ 600 cm^{-1}, which is commonly associated with Cu-O vibrational modes. These Cu-O bands arise from the partial surface oxidation of copper particles during hydrometallurgical processing, ball milling, or exposure to ambient conditions. Such surface oxidation is expected and does not negate the presence of metallic copper within the composite.

Therefore, the FTIR results presented in Fig. 1 confirm the formation of an alumina-based matrix together with the incorporation of copper-containing species within the synthesised composite. The identified vibrational features indicate chemical compatibility between the constituent phases and the development of a structurally stable composite system. These physicochemical characteristics suggest favourable conditions for uniform material deposition and stable interaction with substrate surfaces. The FTIR spectrum shows characteristic absorption bands corresponding to metal–oxygen vibrations and surface functional groups present in the composite.

3.2.2 Ultraviolet–Visible Spectroscopy Absorbance Spectrum of Alumina-Copper Composites

The Ultraviolet (UV) -Visible spectroscopy data of the alumina-copper composite reveal distinct absorbance behaviour across different wavelengths, providing insight into the material's potential applications in coatings and catalysis[36]. As shown in Fig. 2, at 300 nm, the composite exhibits an absorbance of 0.717, indicating significant electronic transitions, possibly due to charge transfer interactions between the alumina and copper phases. This characteristic could enhance the material's ability to absorb UV light, making it suitable for UV-protective coatings. At 540 nm, with an absorbance of 0.327, the composite absorbs less light, which might relate to specific interactions in the visible range. This behaviour could contribute to the material’s aesthetic properties in coating applications, as well as influence its catalytic activity by affecting the surface plasmon resonance of copper nanoparticles. At 720 nm, the composite shows a higher absorbance of 1.183, suggesting strong interactions in the near-infrared region. This could be advantageous in catalytic applications, where the material's ability to absorb and interact with a wide range of wavelengths enhances its effectiveness in processes like photocatalysis or thermal catalysis.

The broad absorbance spectrum across UV, visible, and near-infrared regions suggests that the alumina-copper composite is versatile, with potential for use in both protective coatings and as a catalyst in various chemical reactions. The composite exhibits broad-spectrum light absorption, which not only enhances its protective capabilities but also allows for customizable aesthetic features. Additionally, these optical properties contribute to improved thermal performance. The absorption peaks observed in the UV–visible spectrum correspond to electronic transitions associated with the composite structure.

3.3.3 Importance of X-ray Photoelectron Spectroscopy in Analysing

The X-ray Photoelectron Spectroscopy analysis(XPS), as shown in Fig. 3, provides detailed insight into the surface chemistry of the elemental composition and oxidation states present in the composite surface. The Al 2p/2s spectra confirm that aluminium is predominantly present in the alumina (Al_2O_3) phase, forming a chemically stable and mechanically robust matrix suitable for protective coatings. The Cu 2p spectrum reveals copper primarily in a metallic or low oxidation state, as indicated by the absence of pronounced shake-up satellite peaks typically associated with Cu^{2+} species. This suggests that

copper remains largely unoxidized at the analysed surface depth, which is advantageous for maintaining functional properties such as thermal and electrical conductivity.

The Cu 2p spectrum shown in Fig. 4(a) exhibits characteristic Cu $2p_{3}/_{2}$ and Cu $2p_{1}/_{2}$ peaks at approximately 932.5 eV and 952.3 eV, respectively, without pronounced shake-up satellite features. This indicates that copper is present predominantly in a metallic or low-valence state. The Al 2s spectrum in Fig. 4(b) shows a peak at ~ 119.0 eV, confirming aluminium in the Al^{3+} oxidation state, characteristic of Al_2O_3. The O 1s spectrum presented in Fig. 4(c) is centred at ~ 531.2 eV and corresponds to lattice oxygen associated with Al–O bonding in the alumina matrix. The well-defined O 1s peak indicates that oxygen is strongly bound within the alumina structure rather than existing as loosely adsorbed or reactive surface species. This surface chemistry, dominated by stable Al–O bonding and minimal surface oxidation, reflects a chemically stable surface, which is essential for long-term coating durability and resistance to environmental degradation[25–27][37]. The minor Cu–O features inferred from FTIR are therefore attributed to trace surface oxidation or adsorbed species formed during processing or ambient exposure, which are below the detection limit of XPS and do not indicate the presence of a continuous copper oxide phase.

3.4 THERMAL BEHAVIOUR ANALYSIS - TG-DSC

The thermogravimetric analysis (TGA) shown in Fig. 5(a) reveals multiple stages of mass loss during heating from room temperature to 1000°C. An initial mass loss below 150°C is attributed to the removal of physically adsorbed moisture. A more pronounced mass loss observed between 150°C and 400°C is associated with the decomposition of residual hydroxyl groups and minor organic species introduced during hydrometallurgical processing and ball milling. Beyond 400°C, the mass-loss curve gradually stabilises, with only minor changes observed up to 1000°C, indicating the formation of a thermally stable composite structure.

The limited mass loss at elevated temperatures confirms that the alumina-copper composite maintains structural integrity under high-temperature conditions, a critical requirement for coating materials subjected to thermal cycling. The differential scanning calorimetry (DSC) curve (Fig. 5b) exhibits thermal events corresponding to the mass-loss regions identified in the TGA profile. Endothermic features observed at lower temperatures are associated with moisture removal and dehydration processes. In contrast, broader thermal responses at intermediate temperatures may be linked to structural rearrangements within the alumina matrix. Importantly, the absence of sharp or intense thermal events above 800°C indicates that no major phase transformations or decomposition reactions occur at higher temperatures, further confirming the thermal robustness of the composite[26, 27][38].

Between 600°C and 1000°C, the TG curve shows only minimal mass loss (~ 0.6%), indicating completion of major decomposition and dihydroxylation processes below 600°C. The absence of any sharp weight-loss step confirms that no significant thermal degradation occurs in this region. Similarly, the DSC profile does not exhibit distinct endothermic or exothermic peaks, suggesting the absence of abrupt phase

transitions. The gradual change in heat flow reflects slow structural rearrangement or defect annealing rather than bulk transformation.

3.5 Microstructural Analysis

The High-Resolution Transmission Electron Microscopy (HRTEM) micrographs of the alumina–copper composite at different magnifications (Fig. 6) reveal the formation of agglomerated yet structurally integrated nanoscale particles exhibiting irregular plate-like to clustered morphologies. The primary particles are predominantly distributed within the nanometric regime, while the larger observed features arise from the controlled aggregation of these ultrafine particles driven by their high surface energy. The contrast variation within the micrographs indicates the coexistence of distinct phases, where relatively lighter regions correspond to the alumina matrix, while the darker contrast areas represent copper-rich domains due to the higher electron density of copper. This contrast differentiation confirms the successful incorporation and dispersion of copper within the alumina framework rather than the simple physical mixing of the constituents.

a) 1 µm, b) 0.5 µm, c) 200 nm, d) 500 nm.

At higher magnification (Fig. 6c), the particles display a dense internal structure with well-defined boundaries and the absence of visible microcracks, voids, or structural discontinuities, indicating strong interfacial cohesion between the alumina and copper phases. Such microstructural integrity suggests effective interfacial bonding, which is essential for improving load transfer and enhancing the mechanical and functional performance of the composite material.

Overall, the HRTEM observations confirm the formation of a nanoscale alumina–copper composite structure with uniform particle integration, dense morphology, and stable interfacial characteristics, which are critical factors governing the enhanced physicochemical properties of the synthesised composite. Additionally, the Selected Area Electron Diffraction (SAED) patterns (Fig. 7)provide insights into the crystalline nature of the material, helping to identify phases and assess lattice spacing, which are essential for understanding the composite's microstructure. [27, 39, 40]

The High-Resolution Transmission Electron Microscopy results reveal a well-defined nanostructure with uniform dispersion of alumina and copper phases, indicating strong interfacial bonding and structural stability. Such a refined microstructural configuration is expected to enhance wear resistance, mechanical strength, and overall thermal stability of the composite material.[41–45]

The Selected Area Electron Diffraction patterns obtained from the alumina-copper composite exhibit well-defined concentric diffraction rings, confirming the polycrystalline nature of the material. The diffraction rings were indexed using standard International Centre for Diffraction Data(ICDD) reference data, corresponding to the (220), (311), and (400) crystallographic planes of cubic γ-Al_2O_3 (ICDD PDF No. 10–0425) and the (111) and (200) planes of face-centred cubic metallic copper (ICDD PDF No. 04-0836), confirming the coexistence of crystalline alumina and metallic copper phases. The close agreement between experimental and standard d-values confirms the coexistence of crystalline alumina and copper

phases within the composite. Importantly, no additional diffraction rings attributable to copper oxides, Al-Cu intermetallics, or spinel phases were detected, indicating the absence of detectable interfacial reaction products. This suggests that copper is physically dispersed within the alumina matrix without undergoing chemical transformation during synthesis. The coexistence of these distinct crystalline phases, together with their uniform distribution observed in HR-TEM images, supports a chemically stable composite architecture, which is advantageous for coating applications requiring mechanical integrity, thermal stability, and functional conductivity

The crystalline alumina matrix provides mechanical stability, while the dispersed copper phase contributes functional enhancement. The TEM images reveal the morphology and particle distribution within the alumina–copper composite, while the selected area electron diffraction (SAED) patterns indicate the crystalline nature of the observed phases.[46–48]

3.6 Surface area and porosity Analysis

Surface area and pore structure analyses were conducted to evaluate the textural characteristics of the alumina–copper composite. These parameters are important for understanding the material's adsorption behaviour, pore distribution, and surface accessibility. The analysis was performed using Brunauer–Emmett–Teller (BET) surface area determination, Barrett–Joyner–Halenda (BJH) pore size distribution, Density Functional Theory (DFT) pore analysis, and thickness plot (t-plot) methods. These techniques collectively provide information regarding surface area, pore structure, and the presence of micro- or mesoporous features within the composite material [49].

3.6.1 BJH (Barrett-Joyner-Halenda)

Barrett-Joyner-Halenda (BJH) desorption pore size distribution is presented in Fig. 8, and the cumulative pore volume of the alumina-copper composite is derived from nitrogen adsorption–desorption analysis. The surface area of the composite is 8.731 $m^2 g^{-1}$, with a total pore volume of 0.016 $cm^3 g^{-1}$ and an average pore radius of 20.622 Å, as obtained from the BJH desorption branch. The pore size distribution curve (dV/dlog r) shows that the majority of pores are concentrated in the 10–40 Å range, while the cumulative pore volume (V) increases steadily with increasing pore radius.

In the BJH desorption plot, V represents the cumulative pore volume ($cm^3 g^{-1}$), indicating the total pore volume contributed by pores up to a given radius. The term dV/dlog r represents the differential pore volume distribution, showing how pore volume is distributed across different pore sizes. Peaks in the dV/dlog r curve correspond to dominant pore size ranges within the material.

The observed average pore radius places the composite clearly within the mesoporous regime, which is consistent with alumina-based composites synthesised via hydrometallurgical routes. The moderate surface area and low total pore volume indicate a relatively compact pore structure, which aligns with the dense morphology observed in SEM and HR-TEM analyses. The dominance of mesopores supports controlled diffusion behaviour and structural stability, while avoiding excessive porosity that could

compromise mechanical integrity. When considered together with BET surface area, particle size analysis, and microscopic observations, the BJH results confirm that the composite exhibits a balanced textural structure suitable for applications requiring both surface accessibility and mechanical robustness.

3.6.2 Density Functional Theory

Density Functional Theory (DFT) -derived cumulative pore volume and differential pore volume distribution of the alumina-copper composite as a function of half-pore width are presented in Figs. 9 and 10. The cumulative pore volume curve (V) increases rapidly at lower pore widths and gradually reaches a plateau as the half-pore width approaches approximately 50 Å, indicating that the dominant contribution to pore volume arises from smaller pores. The differential pore volume curve (dV) shows a pronounced distribution within the 10–30 Å range, confirming that mesopores are the prevailing pore type.

In the Density Functional Theory plots, V represents the cumulative pore volume ($cm^3\ g^{-1}$), corresponding to the total pore volume contributed by pores up to a given half-pore width. The dV term denotes the differential pore volume ($cm^3\ g^{-1}\ Å^{-1}$), which describes how pore volume is distributed across different pore sizes. Peaks in the dV curve identify the dominant pore size ranges within the composite.

The Density Functional Theory method summary (Fig. 10) reports a total pore volume of 0.018 $cm^3\ g^{-1}$ and a specific surface area of 7.881 $m^2\ g^{-1}$, which are consistent with the BJH-derived textural parameters. The mode half-pore width of 13.236 Å further confirms that the pore structure is dominated by mesopores. The low fitting error (0.708%) indicates a good agreement between the experimental isotherm data and the Density Functional Theory model, validating the reliability of the analysis. When considered collectively with BET and BJH results, the Density Functional Theory analysis confirms a stable and well-defined pore architecture in the alumina-copper composite

3.6.3 Thickness plot (t-plot) analysis

The Thickness plot (t-plot) analysis (Fig. 11) correlates the statistical thickness (t, Å) of the adsorbed nitrogen layer with the adsorbed gas volume (V, cm^3 STP g^{-1}). The statistical thickness represents the theoretical thickness of the nitrogen film formed on a non-porous reference surface at a given relative pressure (P/P_o), enabling separation of external surface area contributions from pore filling effects. In Fig. 11, the adsorption (A) and desorption (D) data correspond to the experimentally measured nitrogen uptake during the adsorption–desorption cycle at 77 K, while the baseline fit (BF) represents multilayer adsorption on the external surface of the alumina–copper composite. The linear region defined by the BF is used to determine the external surface area. Deviations of the A and D curves from the BF at higher statistical thickness values indicate additional adsorption due to pore filling, confirming the presence of porous structures. The absence of a pronounced negative intercept suggests minimal microporosity, whereas the observed deviations predominantly reflect mesopore-dominated adsorption behaviour. The total pore volume, calculated as 0.01935 $cm^3\ g^{-1}$ for pores smaller than 897.8 Å radius (89.78 nm) at a relative pressure of P/P_o = 0.98920, represents the cumulative contribution of mesopores and larger

accessible pores. These results confirm the porous nature of the composite and are consistent with the BET, BJH, and DFT analyses, collectively validating the reliability of the pore structure evaluation

Overall, the t-plot analysis demonstrates that the alumina-copper composite exhibits a mixed micro-mesoporous structure with mesopore dominance, which is advantageous for coating applications. The presence of mesopores enhances coating adhesion and mechanical interlocking, while the external surface area contributes to improved functional properties such as thermal and electrical conductivity.

3.6.4Brunauer-Emmett-Teller-Specific Surface Area:

The Brunauer-Emmett-Teller (BET) analysis provided a detailed evaluation of the surface area and porosity of the alumina-copper composite using nitrogen adsorption. The nitrogen adsorption isotherms of the alumina-copper composite, displayed in both linear and logarithmic scales, reveal critical insights into the material's porosity and surface area. The linear isotherm shows a gradual increase in nitrogen adsorption as the relative pressure rises, indicating typical mesoporous behaviour with multilayer adsorption followed by capillary condensation. This behaviour is further confirmed in the log-scale plot, where minimal adsorption at very low pressures ($P/P_o < 0.1$) indicates a low presence of micropores, reinforcing that the composite primarily contains mesopores with diameters between 2 and 50 nm.

The data reduction parameters provided in Fig. 9 are additional technical details essential for accurate analysis. Nitrogen was used as the adsorbate with an effective molecular diameter of 3.54 Å, and the experiment was conducted at 77.350 K, nitrogen’s boiling point. The cross-sectional area of a nitrogen molecule (16.200 μ^2) and its liquid density (0.808 g/cc) were utilised in calculating the adsorption volumes. These conditions ensure the reliability of the BET surface area measurements

Table 1
BET-Multipoint Analysis

BET-Multi Point			Explain
1	Slope	234.024	The slope of the BET linear plot is used to determine the surface area by calculating the volume of gas adsorbed at monolayer coverage.
2	Intercept	1.428e + 01	The intercept helps in determining the BET constant (C), which gives insights into the energy of adsorption
3	Correlation Coefficient (r)	0.966523	Indicates the goodness of fit of the linear BET plot. A value of 0.966523 shows a high correlation, ensuring reliability in the calculated surface area.
4	Constant (C)	17.393	Reflects the adsorption energy. A C-value between 10–50, like the 17.393 here, suggests moderate adsorption interactions, typical for mesoporous materials.
5	Surface Area	14.025 m^2/g	The total specific surface area of the alumina-copper composite indicates moderate surface exposure. This value is crucial for assessing the material's potential in catalytic, adsorption, and coating applications

The 14.025 m²/g surface area confirms that in Table 1, the alumina-copper composite has a moderate surface for interaction with gases, liquids, or coatings. This surface area is sufficient for many industrial applications, especially in coatings, where high surface interaction is beneficial for enhanced adhesion and performance[50–52].

The BET and BJH surface area analyses indicate that the composite offers moderate porosity, which enhances the adsorption and adhesion characteristics necessary for coating applications. Compared to typical coating materials, the surface area of 14.025 m²/g provides a notable improvement in performance and durability

4) Conclusion

The present study provides a comprehensive physicochemical evaluation of alumina-copper composites derived from black aluminium dross, with emphasis on assessing their suitability as coating precursor materials through advanced characterisation techniques. The key findings are summarised as follows:

- Structural and chemical analyses using FTIR and XPS confirmed the coexistence of alumina and copper phases, indicating the formation of a chemically stable composite system with well-defined bonding characteristics.
- Thermal analysis (TG-DSC) demonstrated high thermal stability with negligible mass variation at elevated temperatures, confirming that the composite maintains structural integrity up to 1000°C.
- Microstructural investigations using HR-TEM and SAED revealed nanoscale particle morphology with reasonably uniform dispersion and crystalline phase distribution, supporting structural homogeneity of the material.
- Optical characterisation through UV-visible spectroscopy indicated broad spectral absorption behaviour, reflecting stable light–material interaction characteristics of the composite.
- Surface area and porosity analyses (BET, BJH, DFT, and t-plot methods) established the presence of a mesoporous structure with moderate specific surface area and accessible pore networks, which are favourable for surface interaction and coating deposition processes.

Collectively, the thermal, structural, morphological, and surface characterisation results demonstrate that the alumina-copper composite possesses the fundamental physicochemical attributes required for coating precursor materials, including thermal robustness, controlled particle characteristics, and adequate surface accessibility.

The present study establishes the physicochemical suitability of the alumina–copper composite based on comprehensive material characterisation. Future work will focus on coating deposition and quantitative evaluation of mechanical and functional performance, including hardness, adhesion strength, wear resistance, corrosion behaviour, and long-term stability under service conditions, to validate practical applicability in coating systems.

Declarations

Acknowledgment

We also thank Sri Ramakrishna Engineering College for providing the research facilities. The authors also appreciate the support of the DST-SREC Incubation Centre for Recycling Aluminium, which made the project successful.

Funding Declaration

The grant numbers Met4-14/22/2023 Metal-IV from the Ministry of Mines are gratefully received.

Author contributions

Sathiya Seelan G: Conceptualisation, Methodology, Writing - original draft, Visualisation, Project administration.

Bhagyanathan C: Funding acquisition, Supervision, Resources.
Srinath P: Data curation, Writing - review & editing.

Gottmyers Melwyn J: Validation, Investigation, Instrumentation.

Corresponding author

Correspondence to G. Sathiya Seelan.

Conflict of interest

The authors state that there are no conflicts of interest

Data Availability

The datasets used and analysed during the current study are available from the corresponding author on reasonable request.

Ethics Declarations

Ethics Approval and Consent to Participate: Not applicable.

Consent to Publish declaration: not applicable

References

1. Verma SK, Dwivedi VK, Dwivedi SP. 2021. Utilisation of aluminium dross for the development of valuable product–A review. Materials Today: Proceedings, 43, pp.547–550. https://doi.org/10.1016/j.matpr.2020.12.045

2. Sathiyaseelan G, Bhagyanathan C. Utilizing γ- and θ-Alumina from Aluminium Black Dross for Catalytic Applications: Hybrid Sustainable Pyro–Hydrometallurgy and Residue Heat Utilization. Trans Indian Inst Met. 2024. https://doi.org/10.1007/s12666-024-03398-6.
3. Sathiyaseelan G, Bhagyanathan C, Gottmyers Melwyn J, et al. Hydrometallurgical Synthesis of Alumina–Copper Composite Using Waste Black Aluminium Dross for Novel Coating Application. Trans Indian Inst Met. 2025;78:125. https://doi.org/10.1007/s12666-025-03598-8.
4. Meshram A, Jain A, Gautam D, Singh KK. Synthesis and characterization of tamarugite from aluminium dross: Part I. J Environ Manage. 2019;232:978–84. https://doi.org/10.1016/j.jenvman.2018.12.019.
5. Meshram A, Gautam D, Singh KK. Recycling of White Aluminium Dross: Production of Potash Alum. Trans Indian Inst Met. 2020;73:1239–48. https://doi.org/10.1007/s12666-020-01973-1.
6. Hu K, Reed D, Robshaw TJ, Smith RM, Ogden MD. Characterisation of aluminium black dross before and after stepwise salt-phase dissolution in non-aqueous solvents. J Hazard Mater. 2021;123351. https://doi.org/10.1016/j.jhazmat.2020.123351. 401.
7. Zhu X, Yang J, Yang Y, Huang Q, Liu T. Pyrometallurgical process and multipollutant co-conversion for secondary aluminum dross: a review. J Mater Res Technol. 2022;21:1196–211. https://doi.org/10.1016/j.jmrt.2022.09.089.
8. Tripathy AK, Mahalik S, Sarangi CK, Tripathy BC, Sanjay K, Bhattacharya IN. A pyro-hydrometallurgical process for the recovery of alumina from waste aluminium dross. Miner Eng. 2019;137:181–6. https://doi.org/10.1016/j.mineng.2019.04.009.
9. Srivastava A, Meshram A. 2023. A hydrometallurgical perspective of aluminium dross recycling. Materials Today: Proceedings. https://doi.org/10.1016/j.matpr.2023.07.225
10. Shi M, Yu A, Li Y. Production of Alumina from Secondary Aluminum Dross by Hydrometallurgical Process. JOM. 2023;75:291–300. https://doi.org/10.1007/s11837-022-05599-0.
11. da Pereira R, Rosset B, Botelho Junior M, Tenório AB, J.A.S. Development of a Hydrometallurgical Process to Obtain High-Purity Alumina Using Bauxite. In: Wagstaff S, editor. Light Metals 2024. TMS 2024. The Minerals. Metals & Materials Series. Cham: Springer; 2024. https://doi.org/10.1007/978-3-031-50308-5_11.
12. Jach K, Pietrzak K, Wajler A, et al. Fabrication of an Alumina–Copper Composite Using a Ceramic Preform. Powder Metall Met Ceram. 2014;52:680–5. https://doi.org/10.1007/s11106-014-9577-3.
13. Szala M, Łatka L, Walczak M, Winnicki M. Comparative study on the cavitation erosion and sliding wear of cold-sprayed Al/Al2O3 and Cu/Al2O3 coatings, andstainlesssteel,aluminiumalloy,copperandbrass. Metals. 2020;10(7):856. https://doi.org/10.3390/met10070856.
14. Dwivedi SP, Saxena A, Sharma S. Influence of Nano-CuO on Synthesis and Mechanical Behavior of Spent Alumina Catalyst and Grinding Sludge Reinforced Aluminum Based Composite. Inter Metalcast. 2022;16:292–303. https://doi.org/10.1007/s40962-021-00597-5.

15. Beraud C, Courbiere M, Esnouf C, et al. Study of copper-alumina bonding. J Mater Sci. 1989;24:4545–54. https://doi.org/10.1007/BF00544543.
16. Osman A, Elhakeem A, Kaytbay S, Ahmed A. Thermal, electrical and mechanical properties of graphene/nano-alumina/epoxy composites. Mater Chem Phys. 2021;257:123809. https://doi.org/10.1016/j.matchemphys.2020.123809.
17. Akbari MK, Baharvandi HR, Mirzaee O. Fabrication of nano-sized Al2O3 reinforced casting aluminum composite focusing on preparation process of reinforcement powders and evaluation of its properties. Compos Part B: Eng. 2013;55:426–32. https://doi.org/10.1016/j.compositesb.2013.07.008.
18. Beraud C, Courbiere M, Esnouf C, et al. Study of copper-alumina bonding. J Mater Sci. 1989;24:4545–54. https://doi.org/10.1007/BF00544543.
19. Zygmuntowicz J, Maciągowska M, Piotrkiewicz P, et al. Study of the impact of metallic components Cu, Ni, Cr, and Mo on the microstructure of Al2O3–Cu–Me composites. Int J Adv Manuf Technol. 2024;133:5127–46. https://doi.org/10.1007/s00170-024-14070-0.
20. Lowell S, Shields JE, Thomas MA, Thommes M. Characterization of porous solids and powders: surface area, pore size and density. Volume 16. Springer Science & Business Media; 2012. https://doi.org/10.1007/978-1-4020-2303-3.
21. Varvani-Farahani A, Composite Materials. Characterization, Fabrication and Application-Research Challenges and Directions. Appl Compos Mater. 2010;17:63–7. https://doi.org/10.1007/s10443-009-9107-5.
22. Wei D, Dave R, Pfeffer R. Mixing and Characterization of Nanosized Powders: An Assessment of Different Techniques. J Nanopart Res. 2002;4:21–41. https://doi.org/10.1023/A:1020184524538.
23. Angelo PC, Subramanian R, Ravisankar B. Powder metallurgy: science, technology and applications. PHI Learning Pvt. Ltd.; 2022.
24. Ragupathi C, Vijaya JJ, Kennedy LJ, Bououdina M. Nanostructured copper aluminate spinels: Synthesis, structural, optical, magnetic, and catalytic properties. Mater Sci Semiconduct Process. 2014;24:146–56. https://doi.org/10.1016/j.mssp.2014.03.026.
25. Zhu X, Liu W, Zhang H, Zhang H, Zhu J. Narrowing particle size distributions to enhance powder coating performance by improved classifying. Powder Technol. 2024;435:119443. https://doi.org/10.1016/j.powtec.2024.119443.
26. Korotkikh AG, Godunov AB, Sorokin IV. Al–Cu Powder Oxidation Kinetics during Heating in Air. Combust Explos Shock Waves. 2022;58:159–68. https://doi.org/10.1134/S0010508222020046.
27. Hosseini SG, Sheikhpour A, Keshavarz MH, Tavangar S. The effect of metal oxide particle size on the thermal behavior and ignition kinetic of Mg–CuO thermite mixture. Thermochimica acta. 2016;626:1–8. https://doi.org/10.1016/j.tca.2016.01.005.
28. Batista J, Pintar A, Mandrino D, Jenko M, Martin V. XPS and TPR examinations of γ-alumina-supported Pd-Cu catalysts. Appl Catal A. 2001;206(1):113–24. https://doi.org/10.1016/S0926-860X(00)00589-5.

29. Escribano VS, Amores JMG, López EF, et al. Solid state characterization of coprecipitated alumina-gallia mixed oxide powders. J Mater Sci. 2005;40:2013–21. https://doi.org/10.1007/s10853-005-1225-3.
30. De Lucia FC Jr, Giri L, Pesce-Rodriguez RA, Wu CC, Dean SW, Tovar TM, Sausa RC, Wainwright ER, Gottfried JL. Commercial aluminum powders, Part I: Particle size characterization and slow heating rate thermal analysis. PowderTechnology. 2022;399p117162. https://doi.org/10.1016/j.powtec.2022.117162.
31. Kim TG, Raju K, Lee HK. Pressure-less joining of alumina ceramics by the reaction-bonded aluminum oxide (RBAO) method. J Eur Ceram Soc. 2021;41(15):7976–80. https://doi.org/10.1016/j.jeurceramsoc.2021.08.027.
32. Amgalan B, Shiori S, Ichinkhorloo B, Uyanga B, Lee J, Ochirkhuyag B, Choi H. Comparative study of the particle morphology changes in copper powder using various media mills. Geosystem Eng. 2016;20(3):149–62. https://doi.org/10.1080/12269328.2016.1249419.
33. Rahman ML, Islam MS, Ahmed MF, Biswas B, Sharmin N, Neger AT. Extraction and characterization of highly pure alumina (α, γ, and θ) polymorphs from waste beverage cans: A viable waste management approach. Arab J Chem. 2023;16(2):104518. https://doi.org/10.1016/j.arabjc.2022.104518.
34. Dhak D, Pramanik P. Particle size comparison of soft-chemically prepared transition metal (Co, Ni, Cu, Zn) aluminate spinels. J Am Ceram Soc. 2006;89(3):1014–21. https://doi.org/10.1111/j.1551-2916.2005.00769.x.
35. Márquez-Alvarez C, Žilková N, Pérez-Pariente J, Čejka J. Synthesis, characterization and catalytic applications of organized mesoporous aluminas. Catal Reviews. 2008;50(2):222–86. https://doi.org/10.1080/01614940701804042.
36. Korać M, Kamberović Ž, Filipović M. Determination of AL2O3particle sizeinCuAL2O3nanocompositematerialsusingUVspectrophotometry. Metalurgija. 2008;14(4):279–84.
37. Sankar S, Furhan, George A, Ramesan MT. Copper alumina reinforced poly (aniline-co-indole) nanocomposites for optoelectronic devices. Mater Sci Technol. 2023;39(8):941–53. https://doi.org/10.1080/02670836.2022.2152924.
38. Korać M, Kamberović Ž, Anđić Z, Stopić S. Advances in thermochemical synthesis and characterization of the prepared copper/alumina nanocomposites. Metals. 2020;10(6):719. https://doi.org/10.3390/met10060719.
39. Kumar LR, Vijay HM, Krishnaram E, Kumar EN. Consolidation and Characterization of Copper Alumina Composites through Powder Metallurgy. Int J Eng Res Tech (IJERT) ICONNECT. 2018;6(7). https://doi.org/10.3390/MET10060719.
40. Seyedraoufi ZS, Saghafian H, Shabestari SG. Thermochemical synthesis of nanostructured Cu-Al2O3 composite powder. Chem Ind Chem Eng Q. 2014;20(3):339–44. https://doi.org/10.2298/CICEQ120702015S.

41. Wen Y, Huang W, Wang B. A novel method for the preparation of Cu/Al2O3 nanocomposite. Appl Surf Sci. 2012;258(7):2935–8. https://doi.org/10.1016/j.apsusc.2011.11.010.
42. Korać M, Kamberović Ž, Filipović M. Determination of AL2O3particle size in Cu-AL2O3 nanocomposite materials using UV spectrophotometry. Metalurgija. 2008;14(4):279–84.
43. Rakoczy J, Nizioł J, Wieczorek-Ciurowa K, et al. Catalytic characteristics of a copper–alumina nanocomposite formed by the mechanochemical route. Reac Kinet Mech Cat. 2013;108:81–9. https://doi.org/10.1007/s11144-012-0503-8.
44. Saedy S, Haghighi M, Amirkhosrow M. Hydrothermal synthesis and physicochemical characterization of CuO/ZnO/Al2O3 nanopowder. Part I: Effect of crystallization time. Particuology. 2012;10(6):729–36. https://doi.org/10.1016/j.partic.2012.05.001.
45. Mahinroosta M, Allahverdi A. A promising green process for synthesis of high purity activated-alumina nanopowder from secondary aluminum dross. J Clean Prod. 2018;179:93–102. https://doi.org/10.1016/j.jclepro.2018.01.079.
46. Đorđević V, Sredojević DN, Dostanić J, Lončarević D, Ahrenkiel SP, Švrakić N, Brothers E, Belić M, Nedeljković JM. Visible light absorption of surface-modified Al2O3 powders: A comparative DFT and experimental study. Microporous Mesoporous Mater. 2019;273:41–9. https://doi.org/10.1016/j.micromeso.2018.06.053.
47. Gholizadeh Z, Aliannezhadi M, Ghominejad M, et al. High specific surface area γ-Al_2O_3 nanoparticles synthesized by facile and low-cost co-precipitation method. Sci Rep. 2023;13:6131. https://doi.org/10.1038/s41598-023-33266-0.
48. Amini G, Najafpour GD, Rabiee SM, Ghoreyshi AA. Synthesis and Characterization of Amorphous Nano-Alumina Powders with High Surface Area for Biodiesel Production. Chem Eng Technol. 2013;36(10):1708–12. https://doi.org/10.1002/ceat.201300102.
49. Salahudeen N, Ahmed AS, Ala'a H, Dauda M, Waziri SM, Jibril BY, Al-Sabahi J. Synthesis, characterization and adsorption study of nano-sized activated alumina synthesized from kaolin using novel method. Powder Technol. 2015;280:266–72. https://doi.org/10.1016/j.powtec.2015.04.024.
50. Fu L, Li X, Liu M, Yang H. Insights into the nature of Cu doping in amorphous mesoporous alumina. J Mater Chem A. 2013;1(46):14592–605.
51. Bardestani R, Patience GS, Kaliaguine S. Experimental methods in chemical engineering: specific surface area and pore size distribution measurements—BET, BJH, and DFT. Can J Chem Eng. 2019;97(11):2781–91. https://doi.org/10.1002/cjce.23632.
52. Huang B, Bartholomew CH, Woodfield BF. Improved calculations of pore size distribution for relatively large, irregular slit-shaped mesopore structure. Microporous Mesoporous Mater. 2014;184:112–21. https://doi.org/10.1002/cjce.23632.

Figures

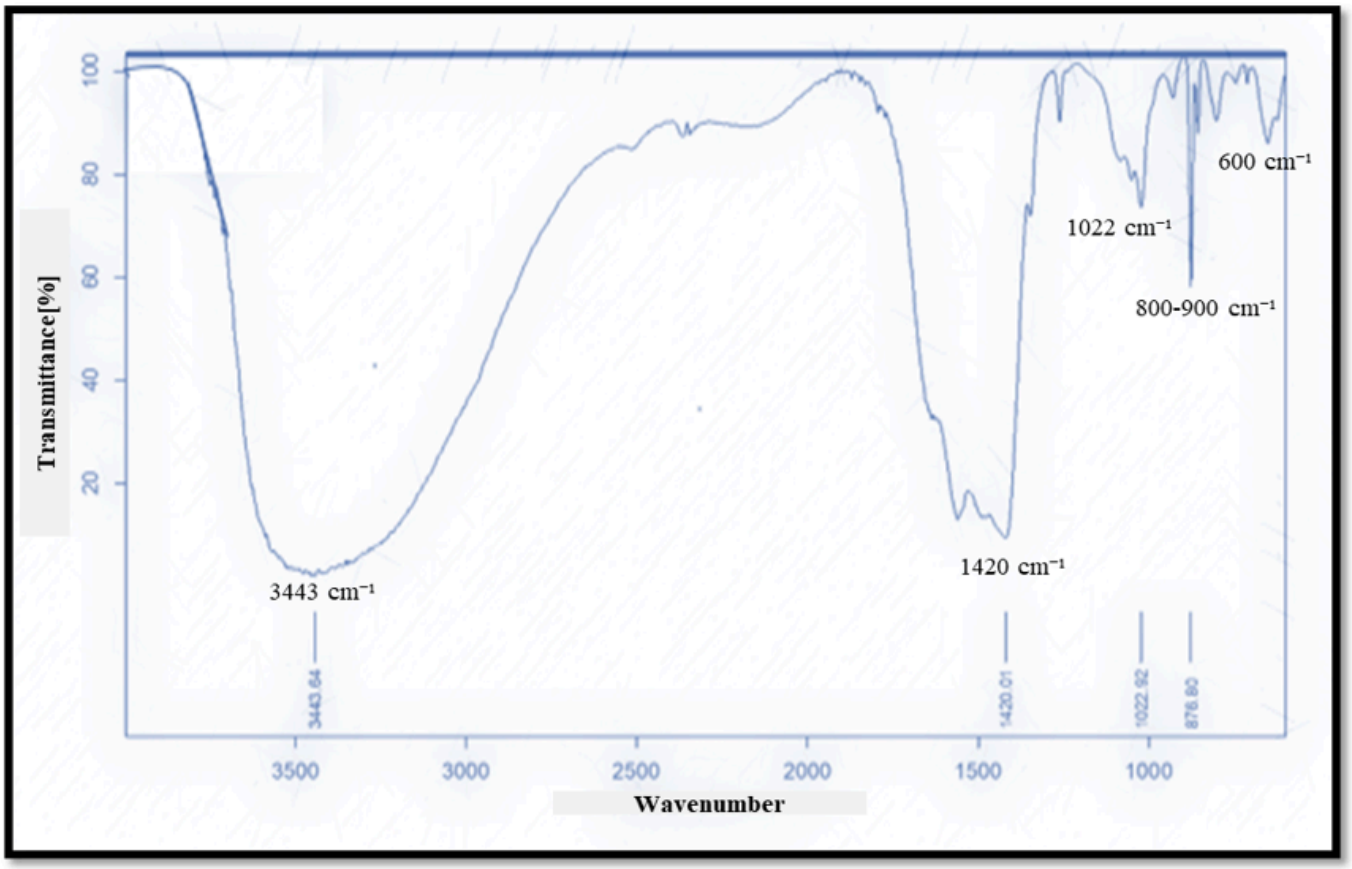


Figure 1

FTIR spectrum of the synthesised alumina-copper composite.

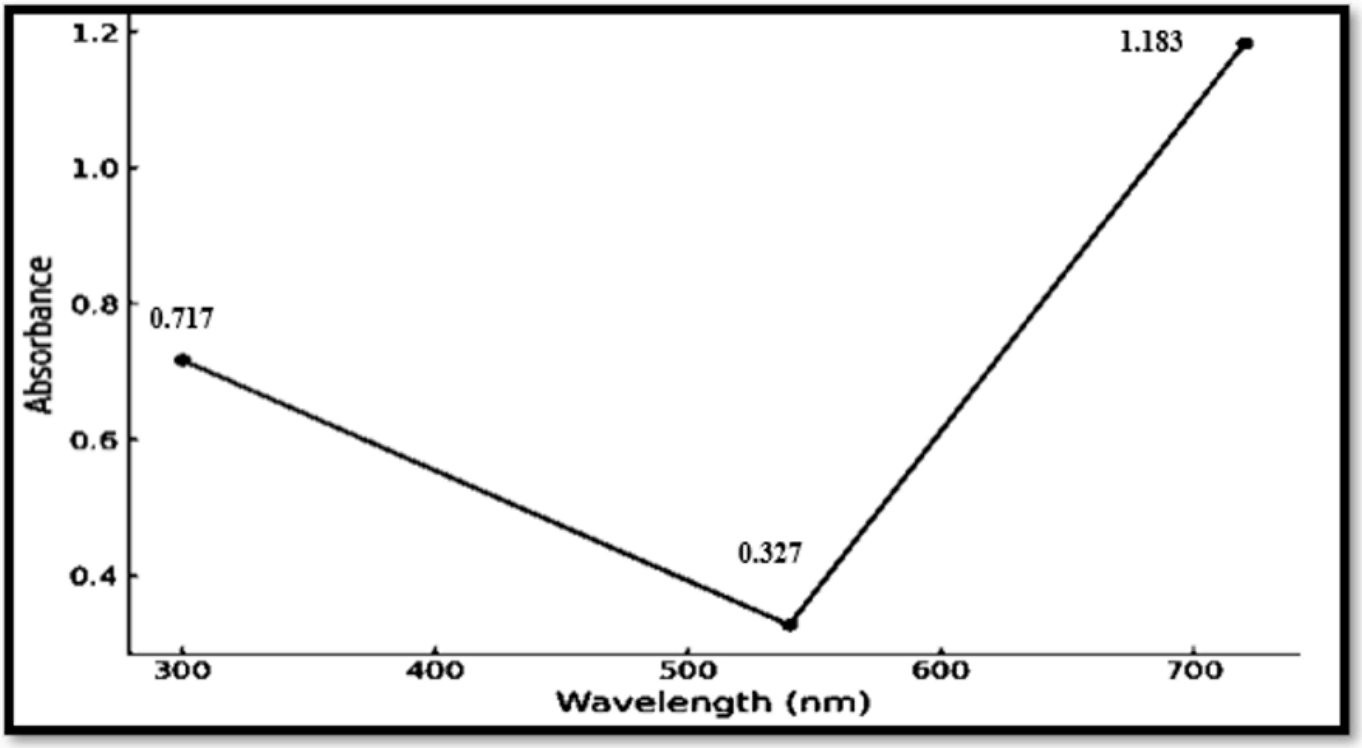


Figure 2

UV-Visible absorption spectrum of the synthesized alumina-copper composite

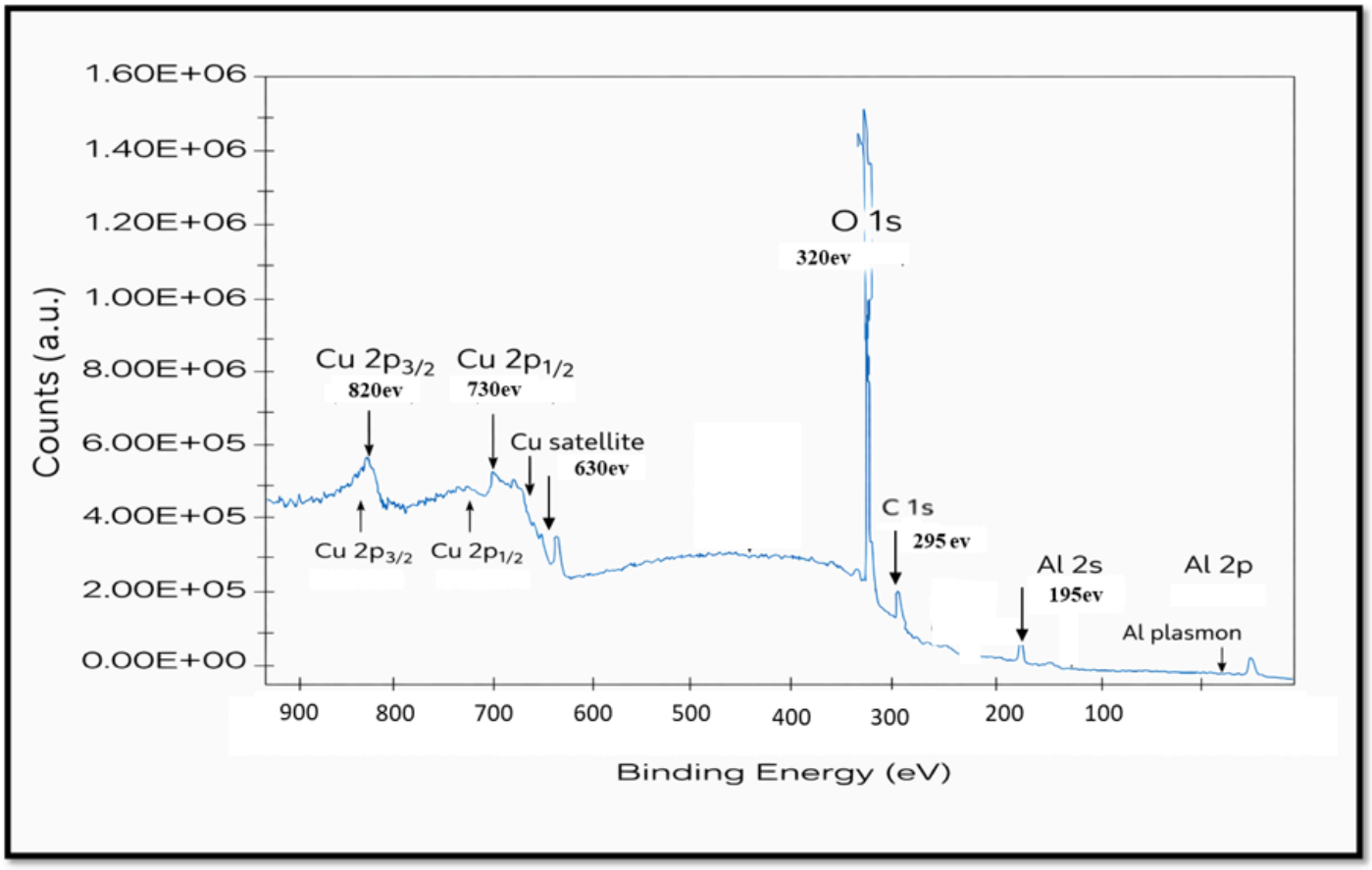


Figure 3

XPS survey spectrum of the Al_2O_3–Cu composite,

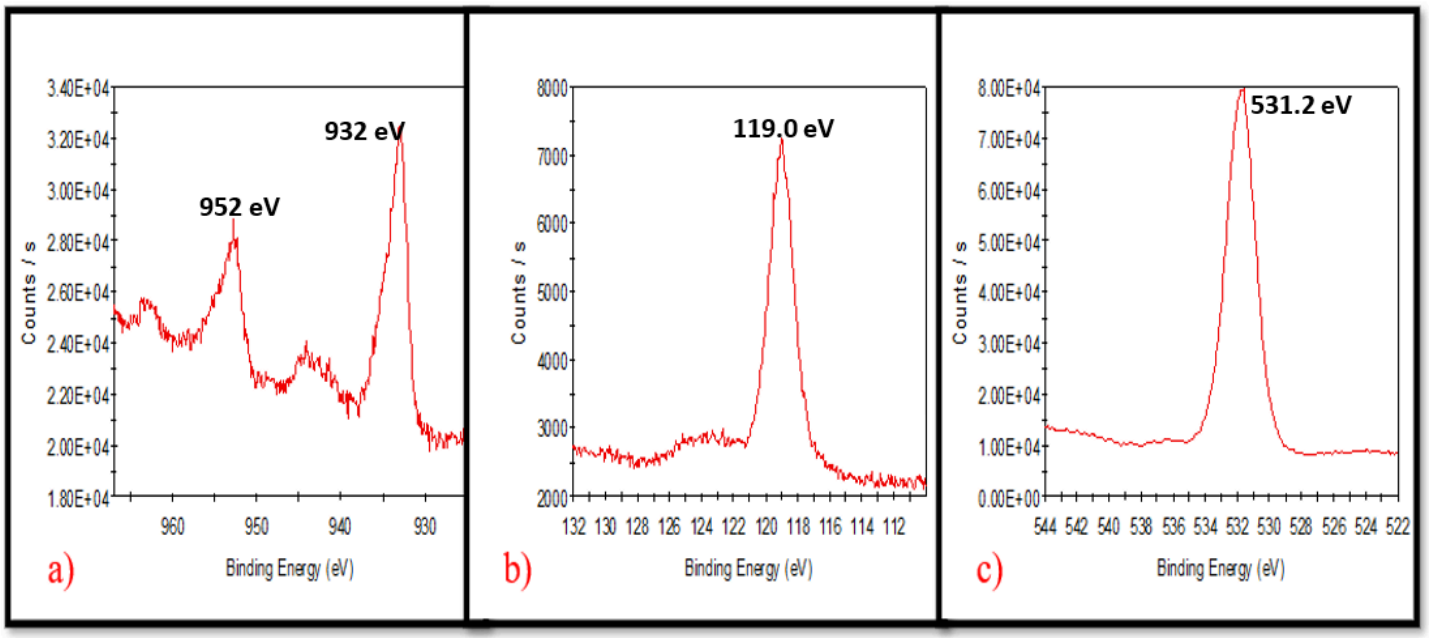


Figure 4

(a) Cu 2p, (b) Al 2s, and (c) O1s

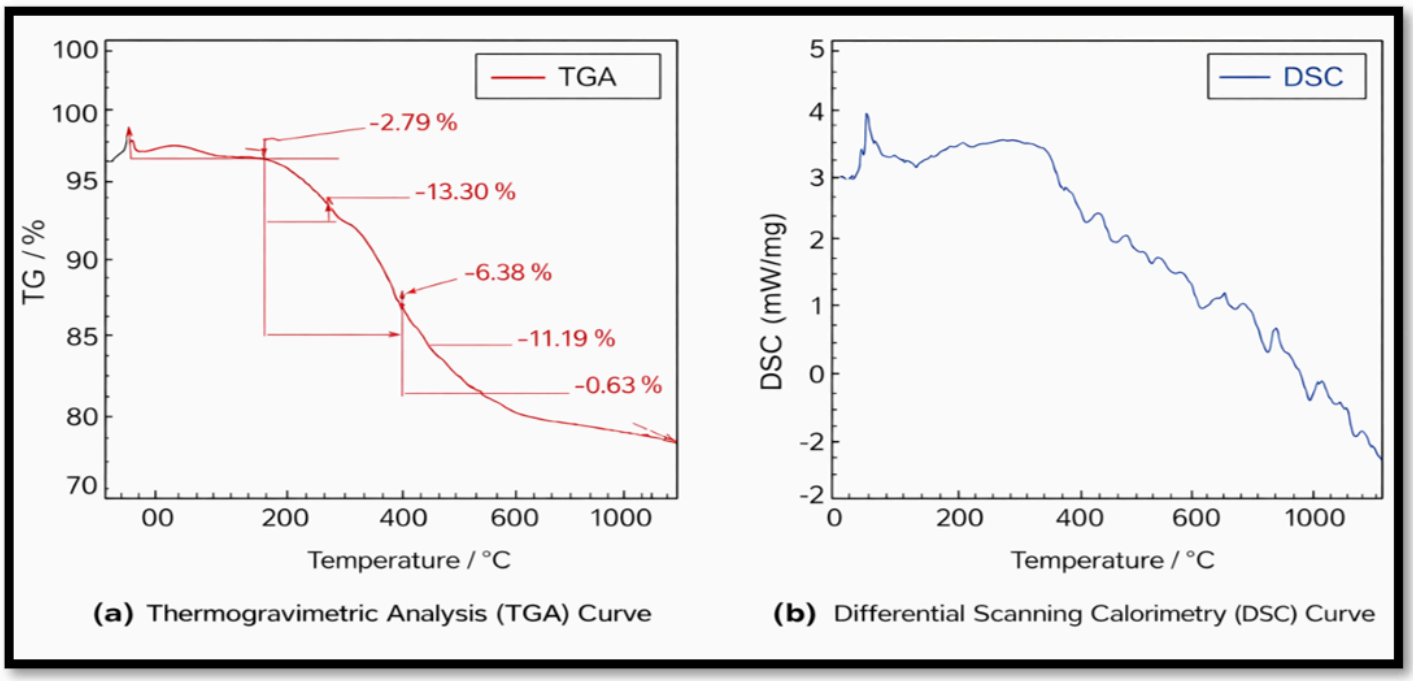


Figure 5

(a) Thermogravimetric analysis (TGA), (b) differential scanning calorimetry (DSC) Analysis of Composite

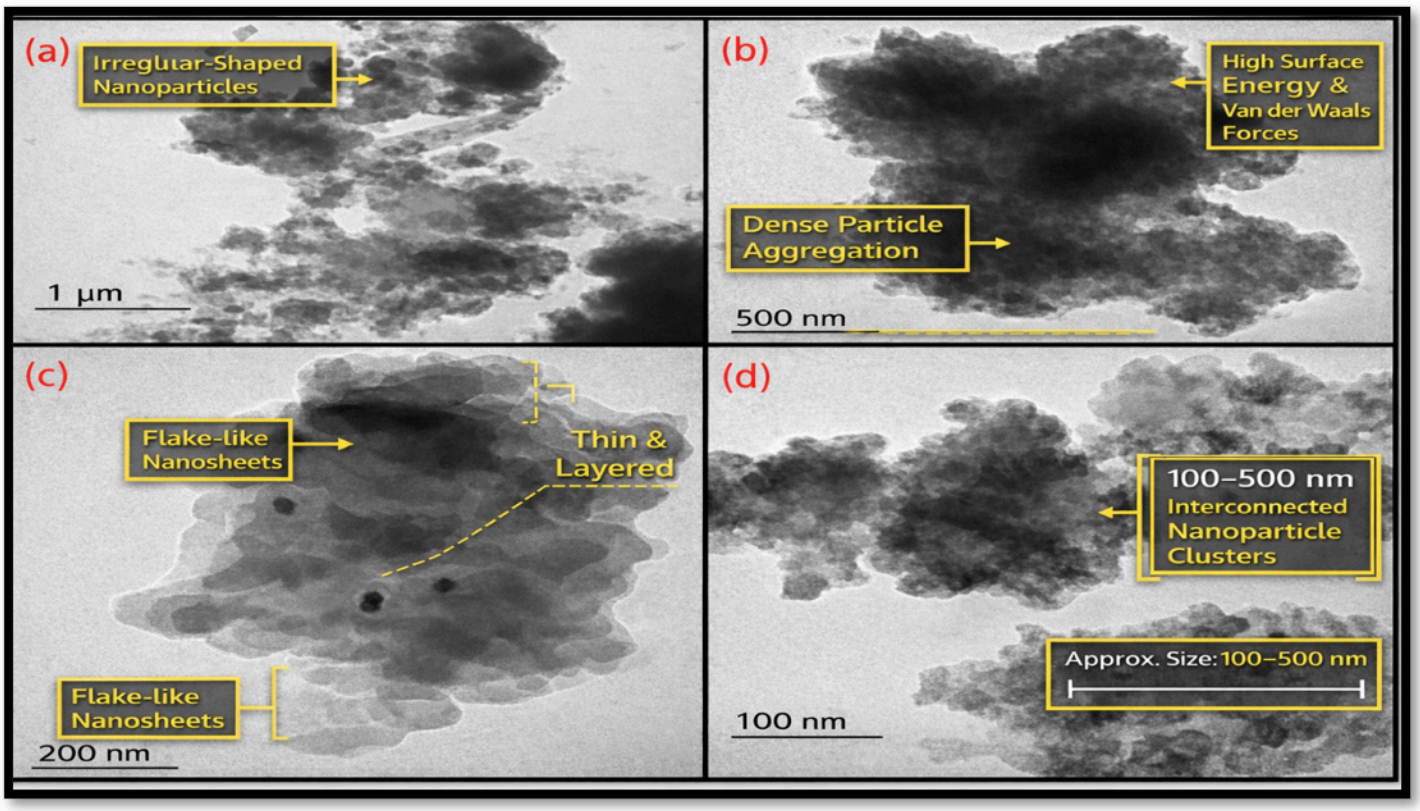


Figure 6

HR-TEM bright field images at different scales

a) 1 µm, b) 0.5 µm, c) 200 nm, d) 500 nm.

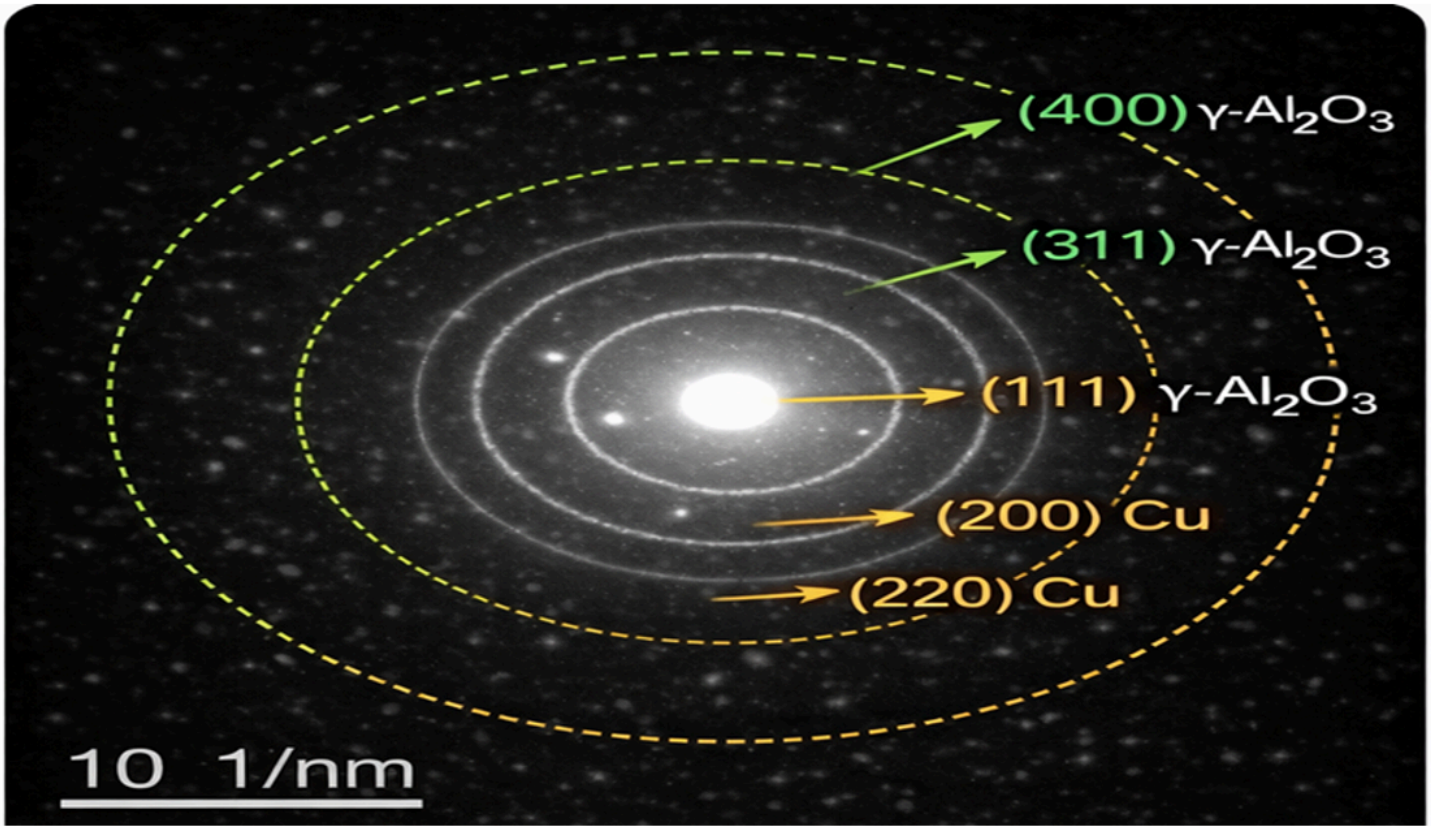


Figure 7

SAED pattern of the alumina-copper composite

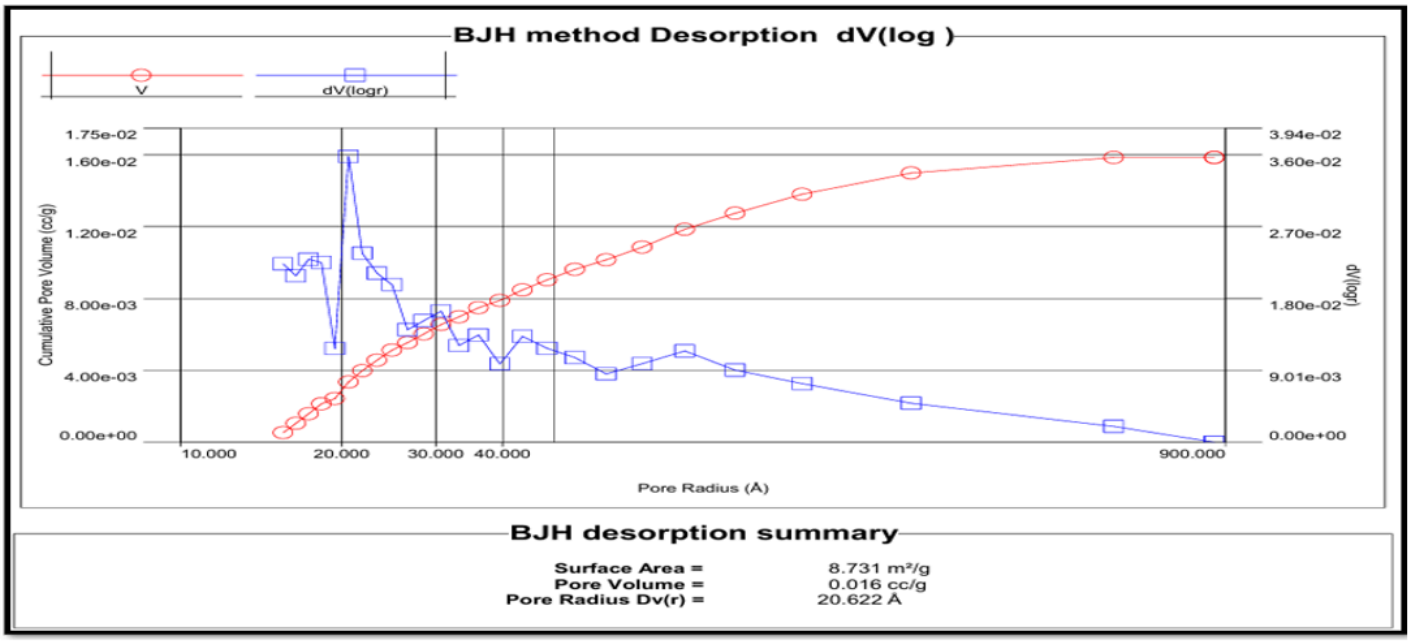


Figure 8

BJH desorption pore size distribution and cumulative pore volume of the alumina-copper composite obtained from nitrogen adsorption-desorption measurements at 77 K.

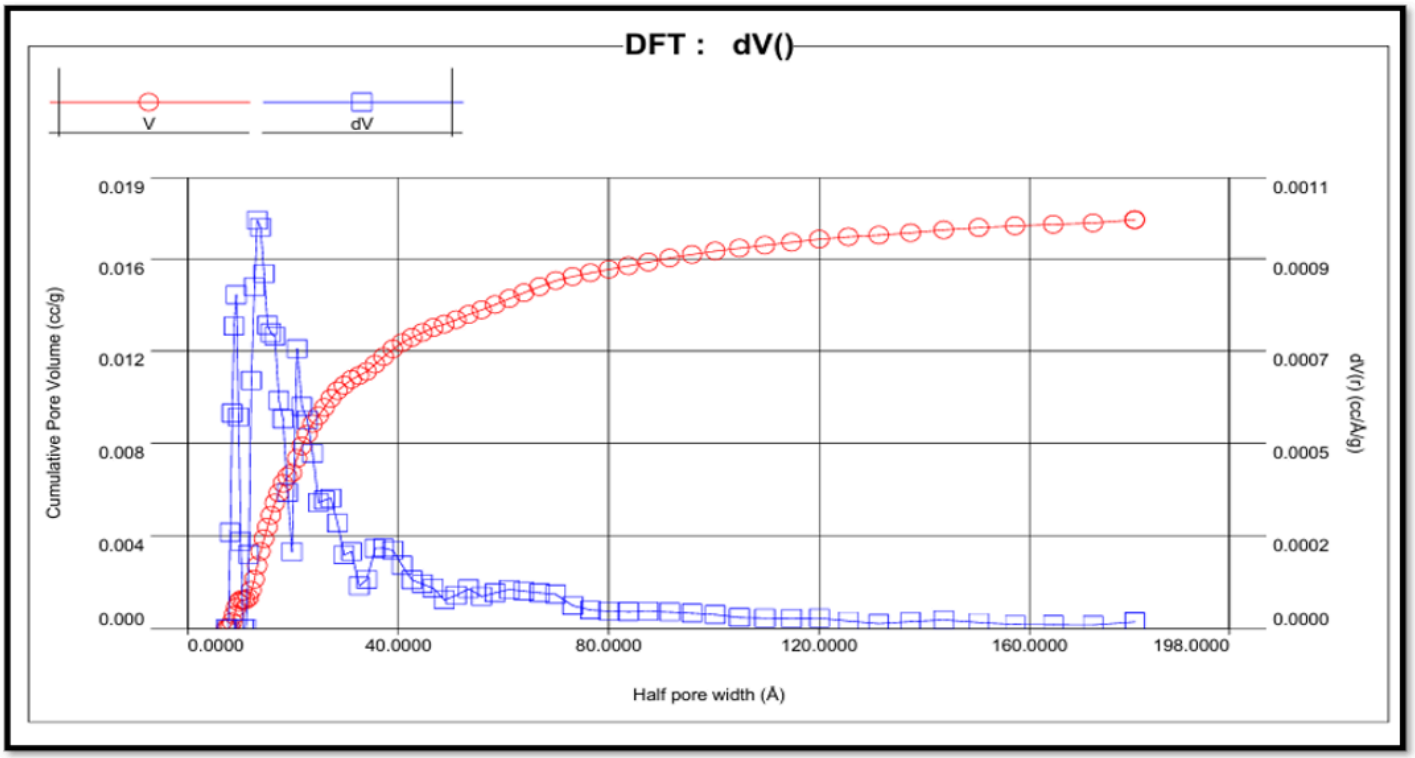


Figure 9

DFT pore size analysis of the alumina-copper composite derived from nitrogen adsorption-desorption data at 77 K

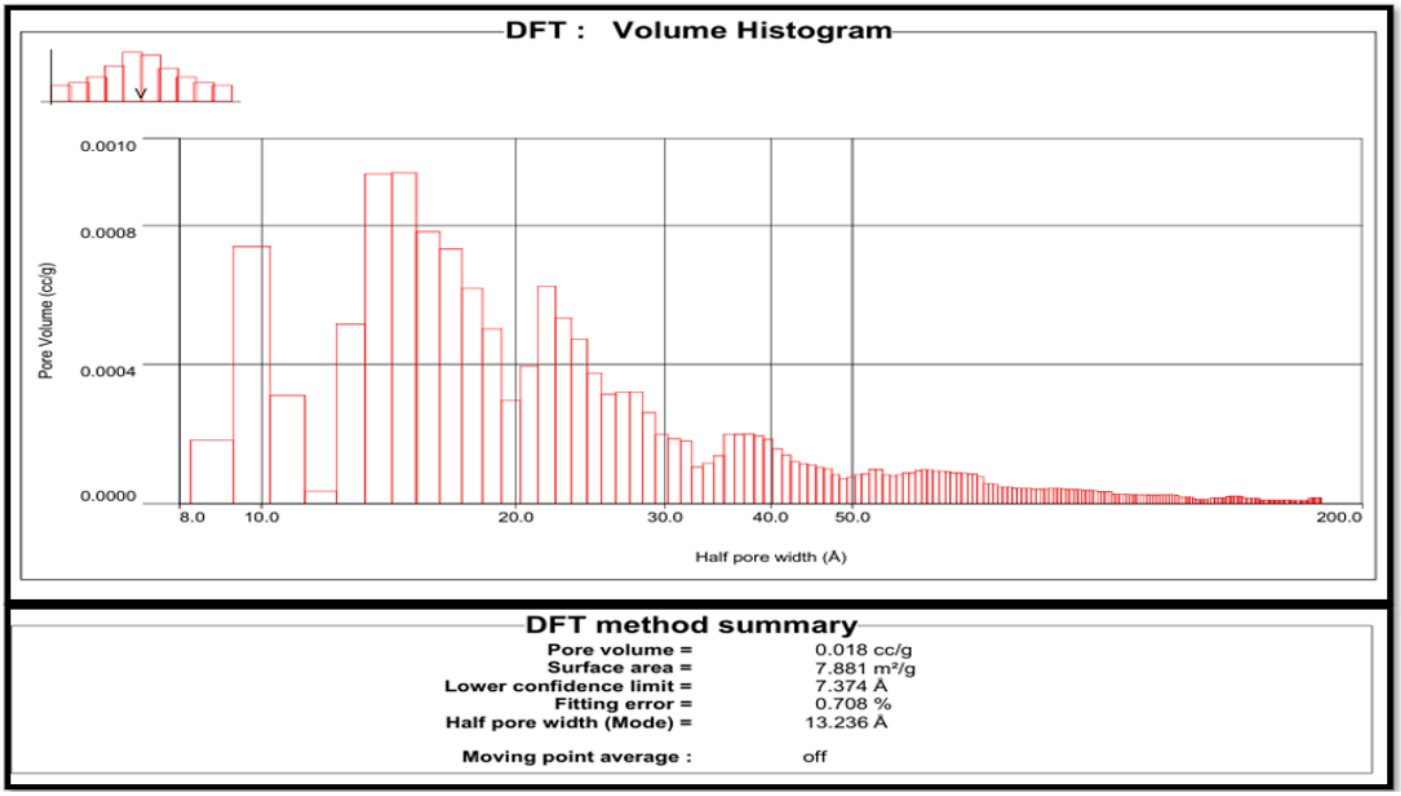


Figure 10

DFT method summary for the alumina-copper composite, obtained from nitrogen adsorption-desorption analysis.

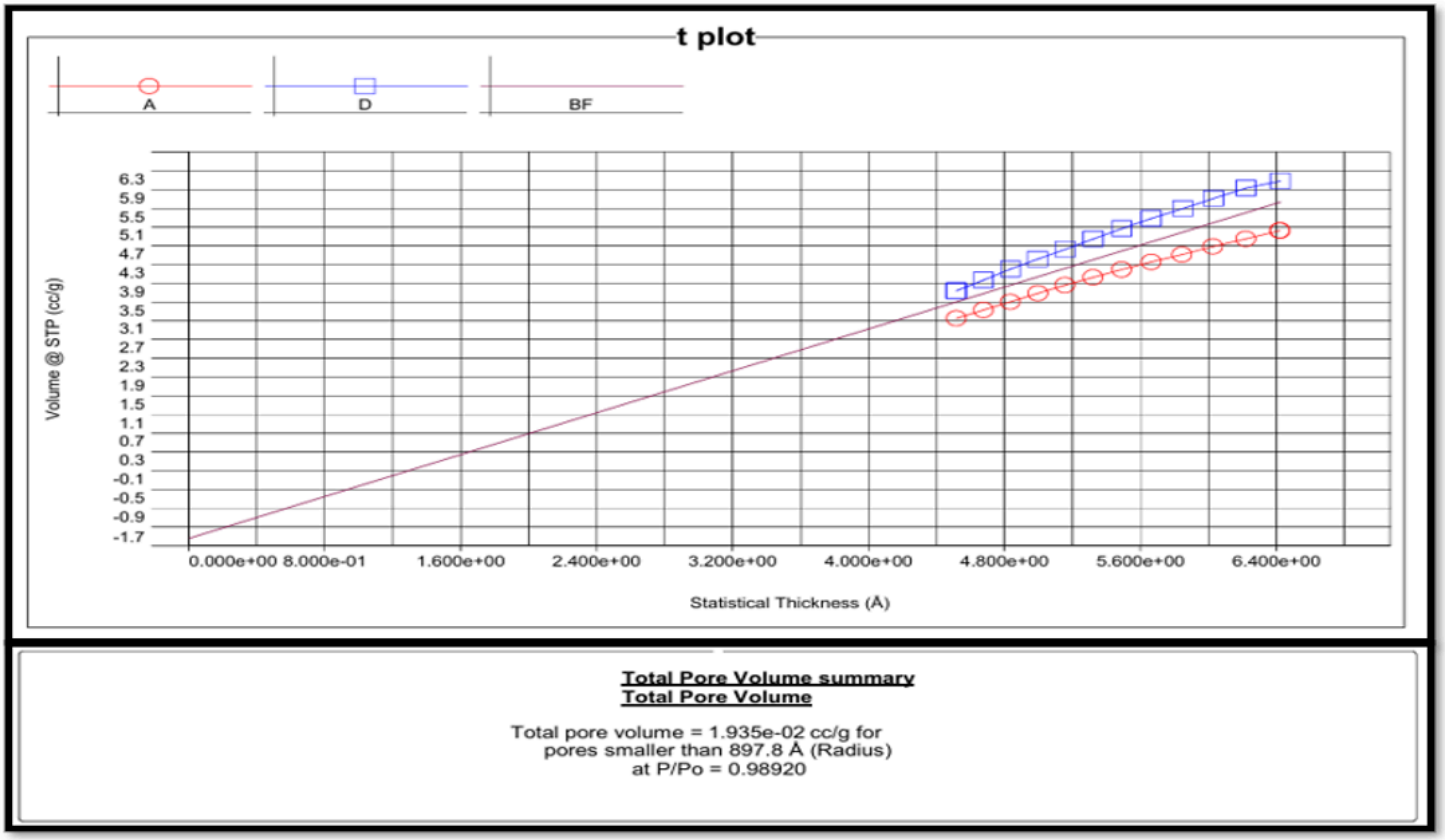


Figure 11

Pour t-plot analysis of the alumina-copper composite derived from nitrogen adsorption-desorption isotherms at 77 K.

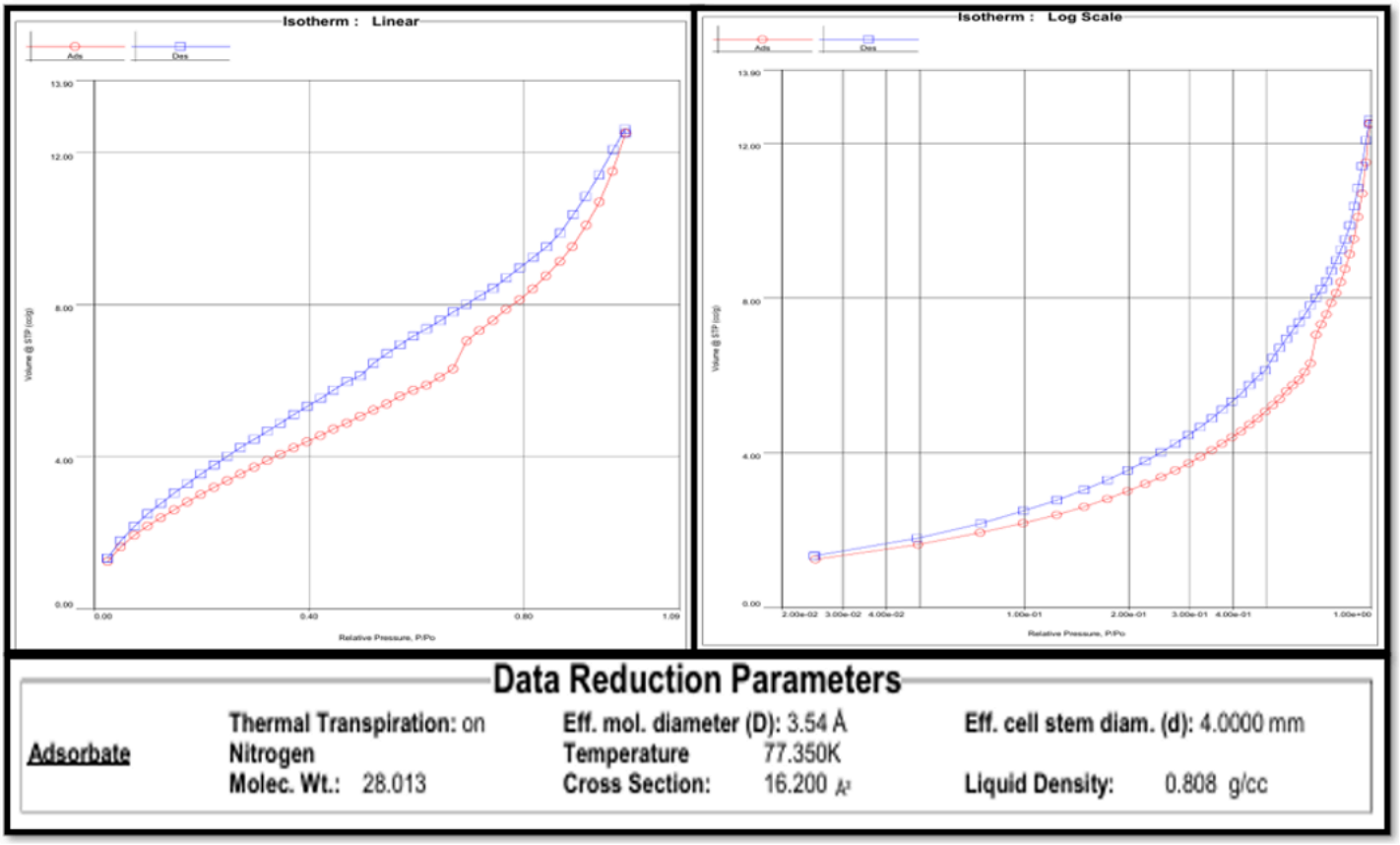


Figure 12

BET specific surface area analysis of the alumina-copper composite obtained from nitrogen adsorption–desorption measurements at 77 K